Draft version 2024.3.12.1140
Typeset using LaTeX **preprint** style in AASTeX631

Supplementary Material for Sensitivity of Polarization to Grain Shape: II. Aggregates

B. T. Draine [1, 2]

[1] *Dept. of Astrophysical Sciences, Princeton University, Princeton, NJ 08544, USA*
[2] *Institute for Advanced Study, Princeton, NJ 08540, USA*

ABSTRACT

Visualizations of the full set of aggregate shapes studied in the paper "Sensitivity of Polarization to Grain Shape: II. Aggregates", and wavelength dependence of extinction and polarization cross sections for every shape.

Keywords: interstellar dust (836), radiative transfer (1335)

1. INTRODUCTION

As described in Paper II (Draine 2024a), scattering and absorption cross sections have been calculated for a total of 45 targets. 42 of these targets were irregular aggregates nominally consisting of $N = 256$ equal-size spheres[1] generated using twelve different procedures. Paper II included images of one example of each type. Here we provide views of all 45 aggregates.

Paper II included figures showing the extinction and polarization cross sections as a function of wavelength λ for one example of each type. Here we provide figures showing the extinction and polarizations for every aggregate, for completeness.

2. AGGREGATES

All targets are assemblies of equal-sized spheres. Targets studied include $N = 2$ ("bisphere", two touching spheres), two $N = 3$ examples ("trisphere" and "threesphere" geometry), and 42 $N = 256$ examples, generated by a total of nine different procedures.

Three of the procedures are the "BA". "BAM1", and "BAM2" random aggregation procedures described by Shen et al. (2008). In addition, Paper II discusses modification of these random aggregates to greater degrees of flattening or elongation by random aggregation followed by three different "trimming" procedures, denoted *trimA*, *trimB*, and *trimC* (see Paper II).

Figure 1 shows the $N = 2$ and $N = 3$ examples. Figures 2–11 show the $MN = 256$ aggregates studied.

Each of the targets in Paper II is shown from three orientations. Axis $\hat{\boldsymbol{a}}_1, \hat{\boldsymbol{a}}_2, \hat{\boldsymbol{a}}_3$ are the principal exes of largest, intermediate, and smallest moments of inertia. In perfect spinning alignment (PSA), the grain is spinning around $\hat{\boldsymbol{a}}_1$, and radiation in propagating perpendicular to $\hat{\boldsymbol{a}}_1$.

draine@astro.princeton.edu

[1] As explained in Paper II, one of the aggregates consisted of only $N = 203$ spheres as a result of the "trimming" procedure used.

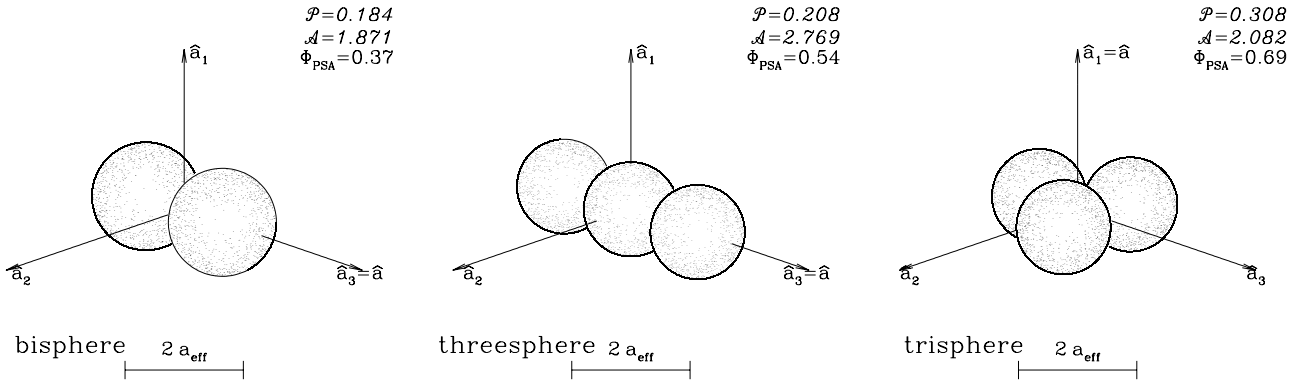

Figure 1. Bisphere, threesphere, and trisphere geometries. The scale bars show $2a_{\rm eff}$, the diameter of an equal-volume sphere. $\hat{\boldsymbol{a}}_1$ is the principal axis of largest moment of inertia; grains are asssumed to spin around this axis.

3. CROSS SECTIONS FOR EXTINCTION AND POLARIZATION

As described in Papers I and II, cross sections for absorption and scattering have been calculated for all of shapes in this study, for selected sizes $a_{\rm eff} = 0.05, 0.10, 0.15, 0.20, 0.25, 0.30\mu$m, and 251 wavelengths $\lambda \in [0.1\mu{\rm m}, 100\mu{\rm m}]$.

The computations were done using the discrete dipole approximation (DDA) code `DDSCAT`[2]. Calculations were carried out using different numbers $N_{\rm dip}$ of dipoles to represent the target; the computed results are used to extrapolate to $N_{\rm dip} \to \infty$, using Eq. (8) in Draine (2024b).

Uncertainties in the extrapolation are estimated by using calculations for three different $N_{\rm dip}$ [][Eq. 9](Draine 2024b).

For all of the shapes studied in Paper II, Figures 14–25 show the dimensionless quantities $\lambda Q_{\rm ran}/a_{\rm eff}$ and $\lambda Q_{\rm pol,PSA}/a_{\rm eff}$, where $Q_{\rm ran}$ is the efficiency factor for extinction by randomly-oriented targets, and $Q_{\rm pol,PSA}$ is the efficiency factor for polarization by particles in perfect spinning alignment.

$Q_{\rm ran}(\lambda)$, $Q_{\rm pol,PSA}(\lambda)$ and $Q_{\rm sca}(\lambda)$ obtained by extrapolation are available in machine-readable form over the full wavelength range 0.1–100μm at xxx *[btd note: doi]*.

The `DDSCAT` parameter files used for these calculations are available at *url here*. Additional data are available from the author upon request.

1 This work was supported in part by NSF grant AST-1908123. I thank Robert Lupton for availability
2 of the SM package.

REFERENCES

Draine, B. T. 2024a, in prep.
—. 2024b, ApJ, accepted; arXiv:2310.15229
Shen, Y., Draine, B. T., & Johnson, E. T. 2008, ApJ, 689, 260, doi: 10.1086/592765

[2] DDSCAT 7.3.3, available from www.ddscat.org

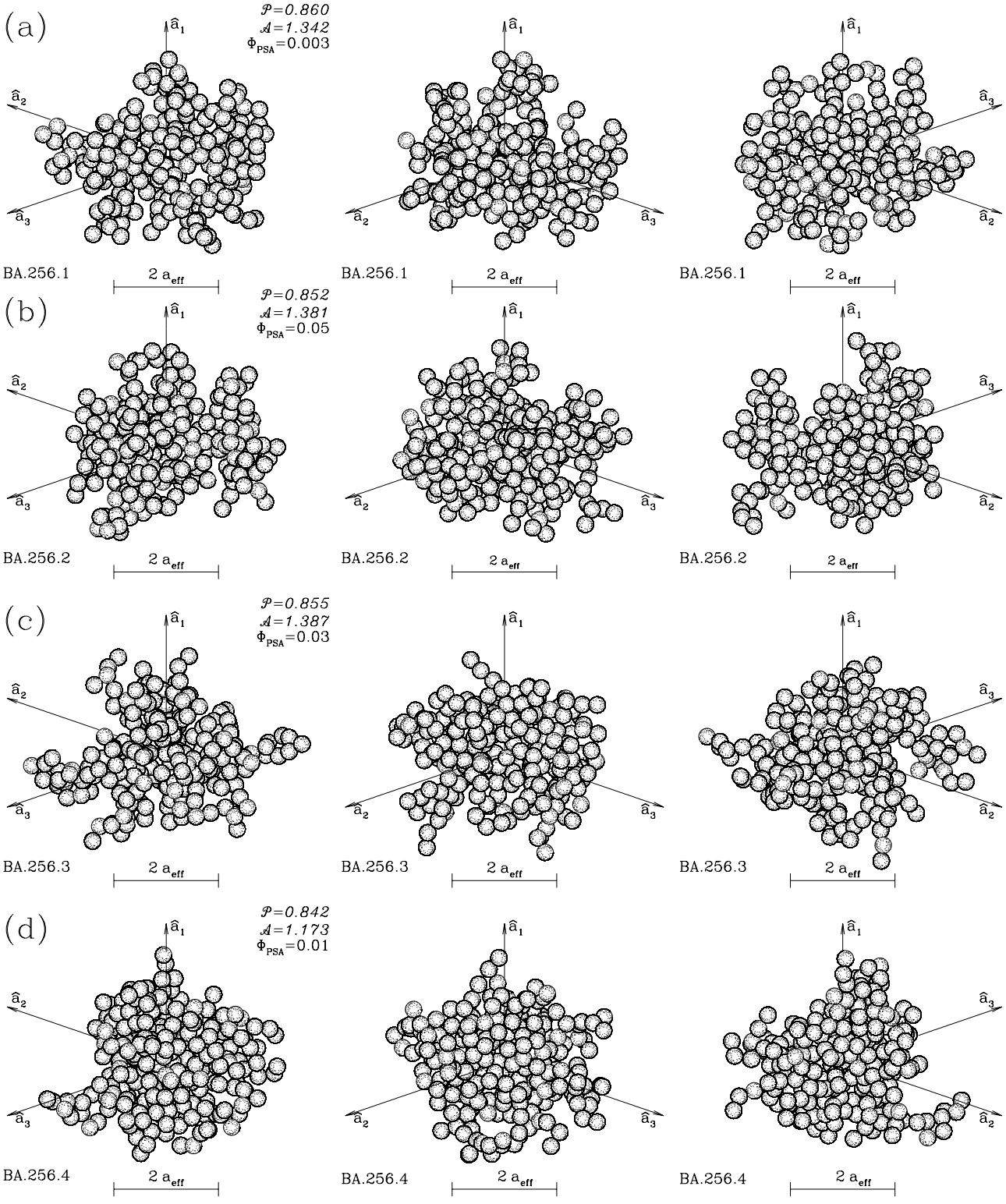

Figure 2. $N = 256$ BA random aggregates.

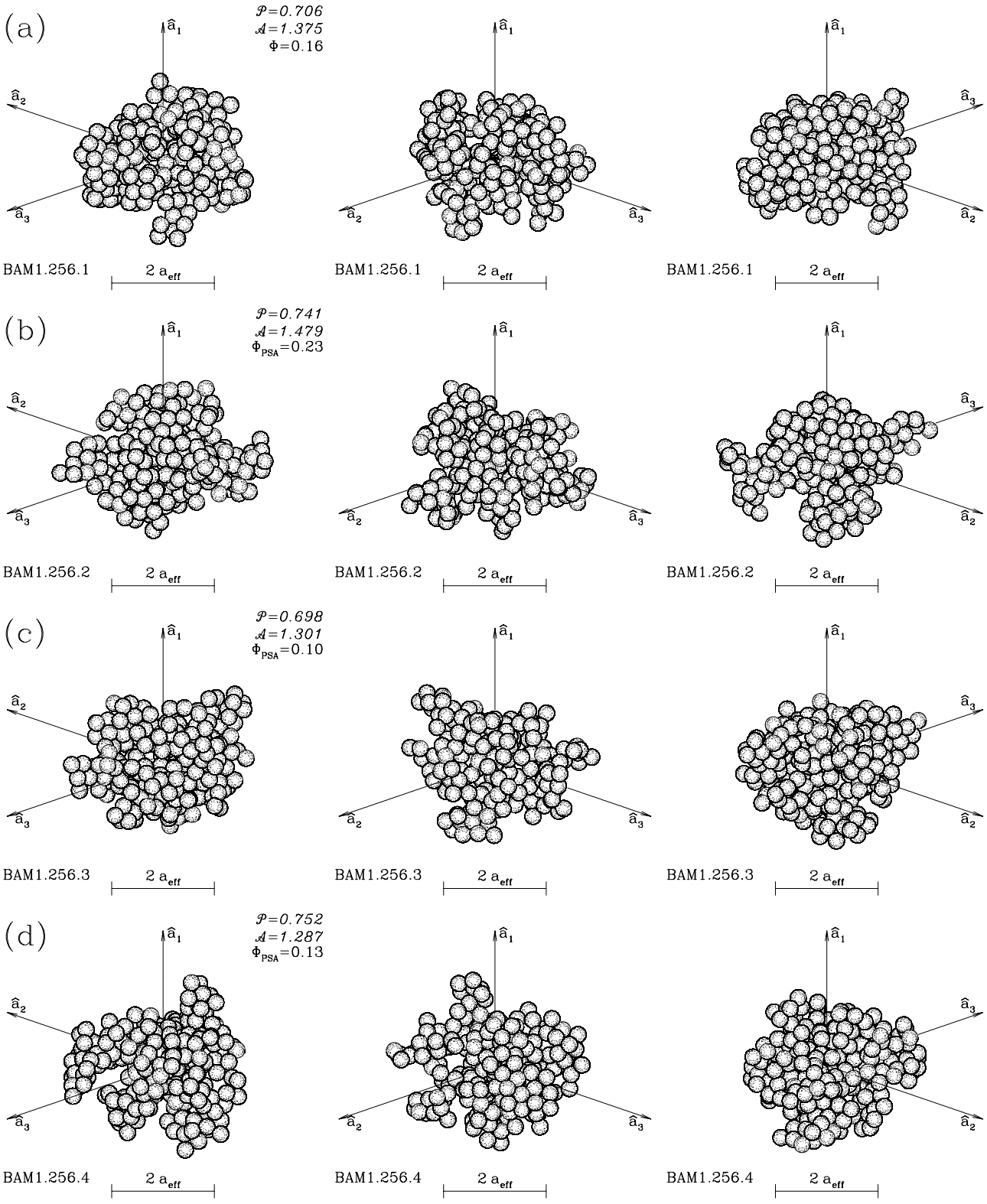

Figure 3. $N = 256$ BAM1 random aggregates.

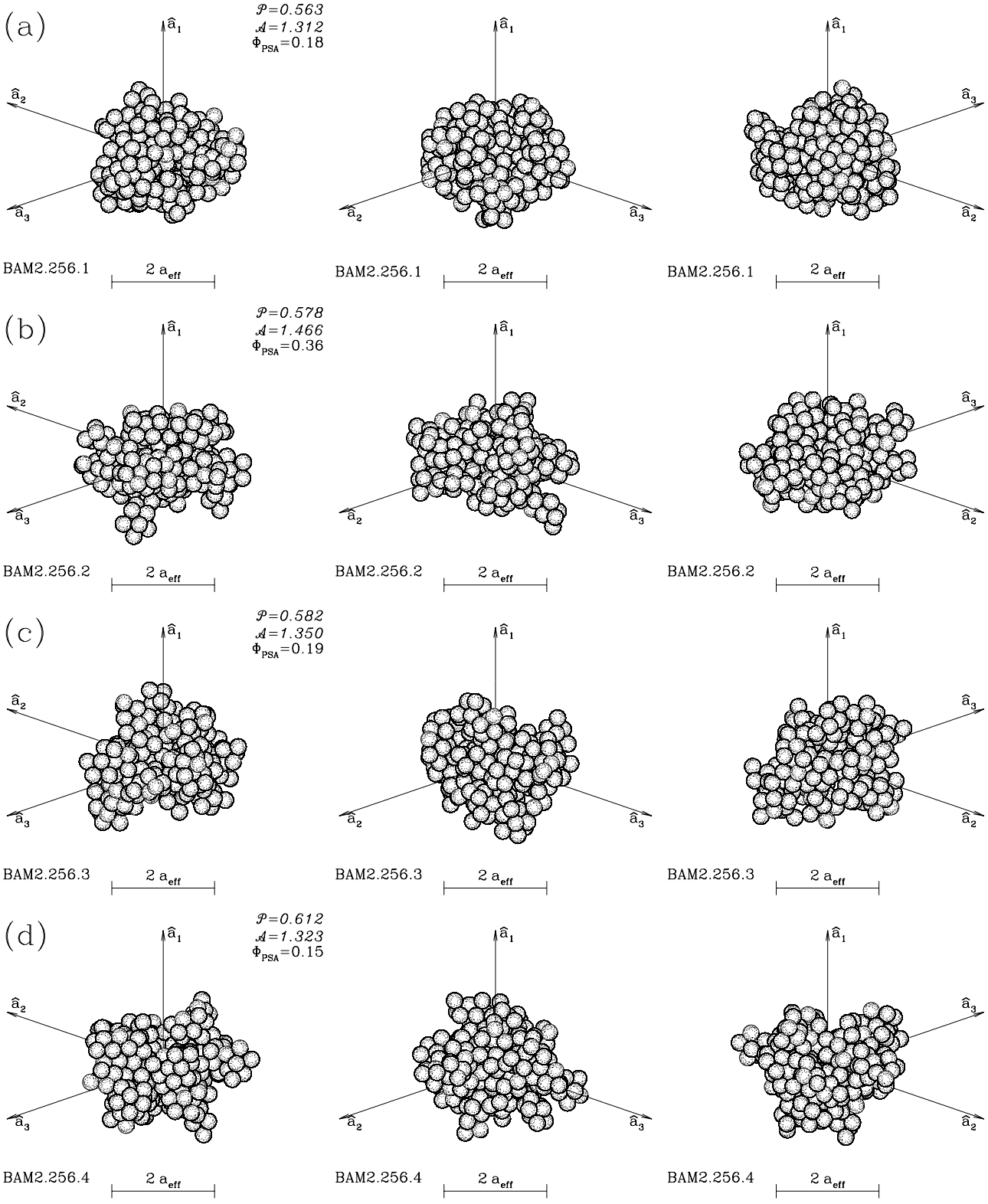

Figure 4. $N = 256$ BAM2 random aggregates.

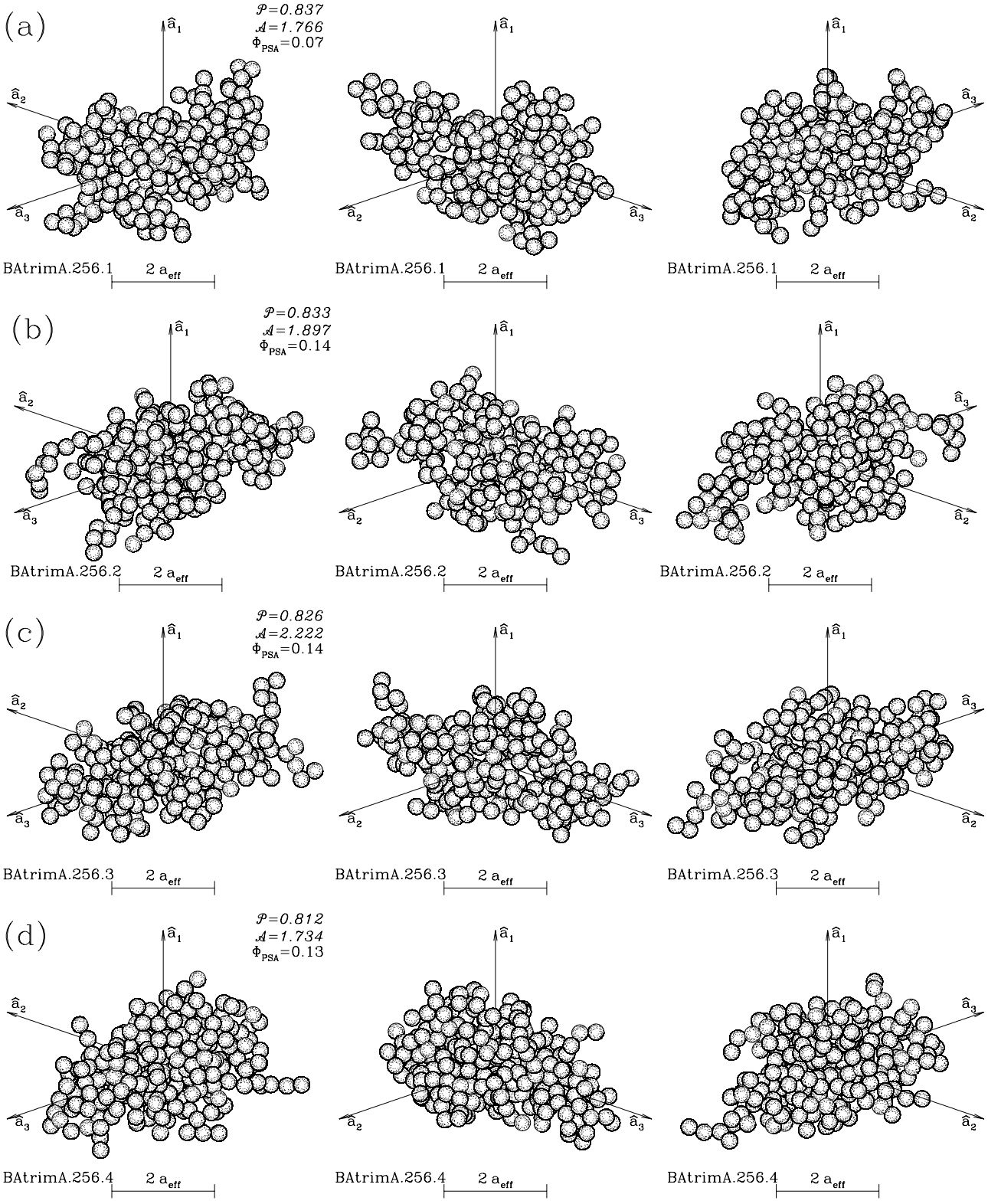

Figure 5. $N = 256$ aggregates obtained from $N = 512$ BA clusters modified by the *trimA* procedure.

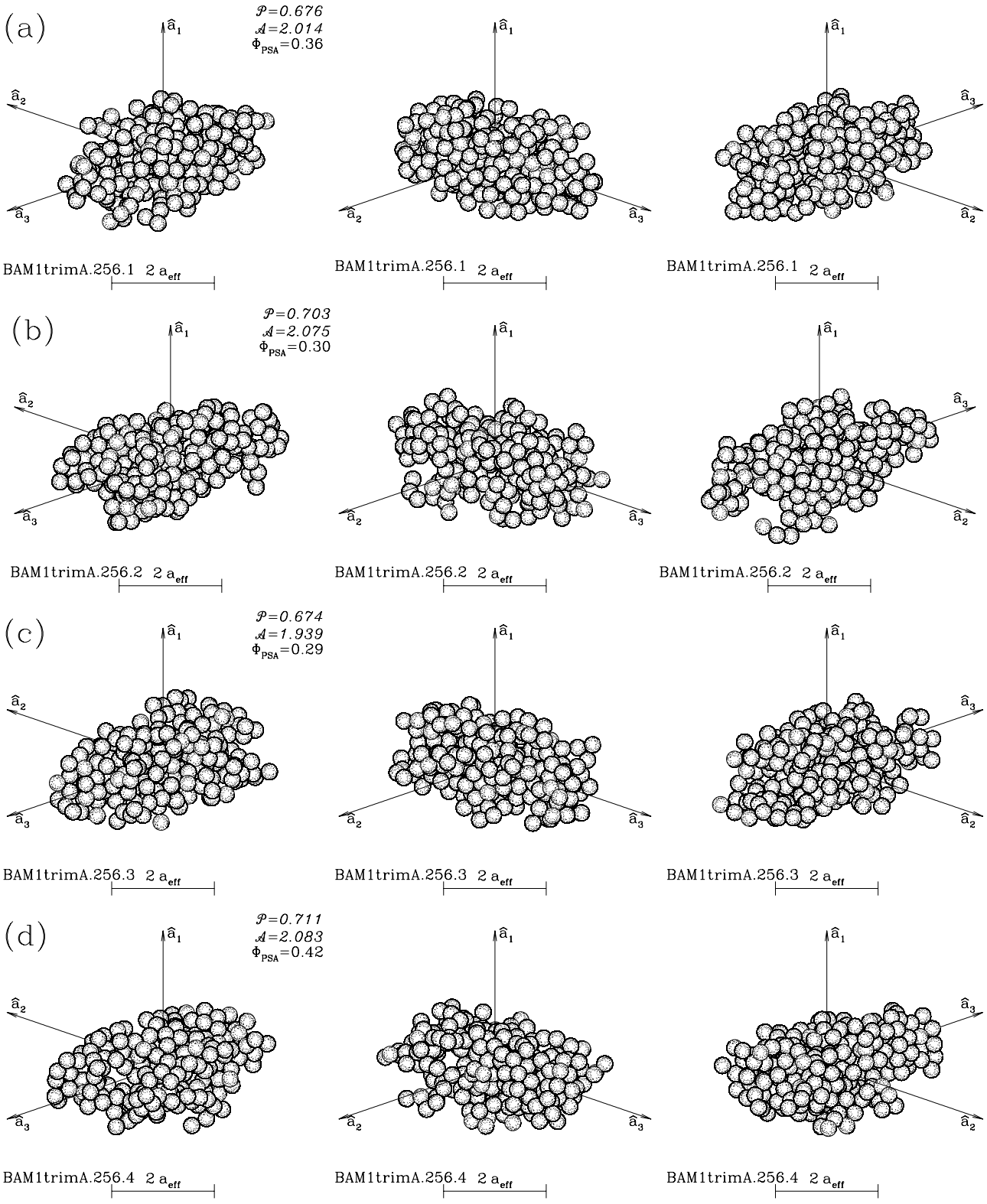

Figure 6. $N = 256$ aggregates obtained from $N = 512$ BAM1 clusters modified by the *trimA* procedure.

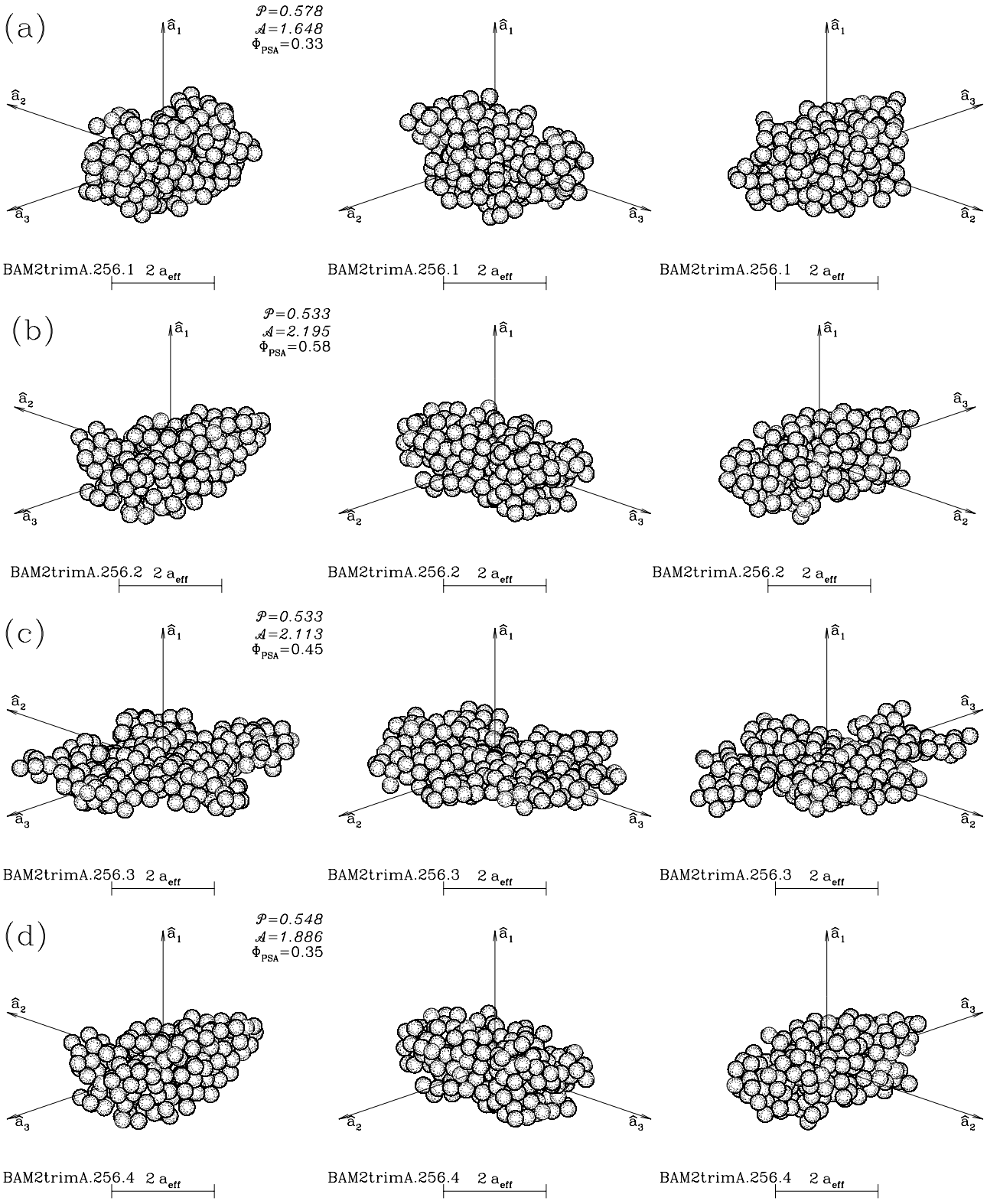

Figure 7. $N = 256$ aggregates obtained from $N = 512$ BAM2 clusters modified by the *trimA* procedure.

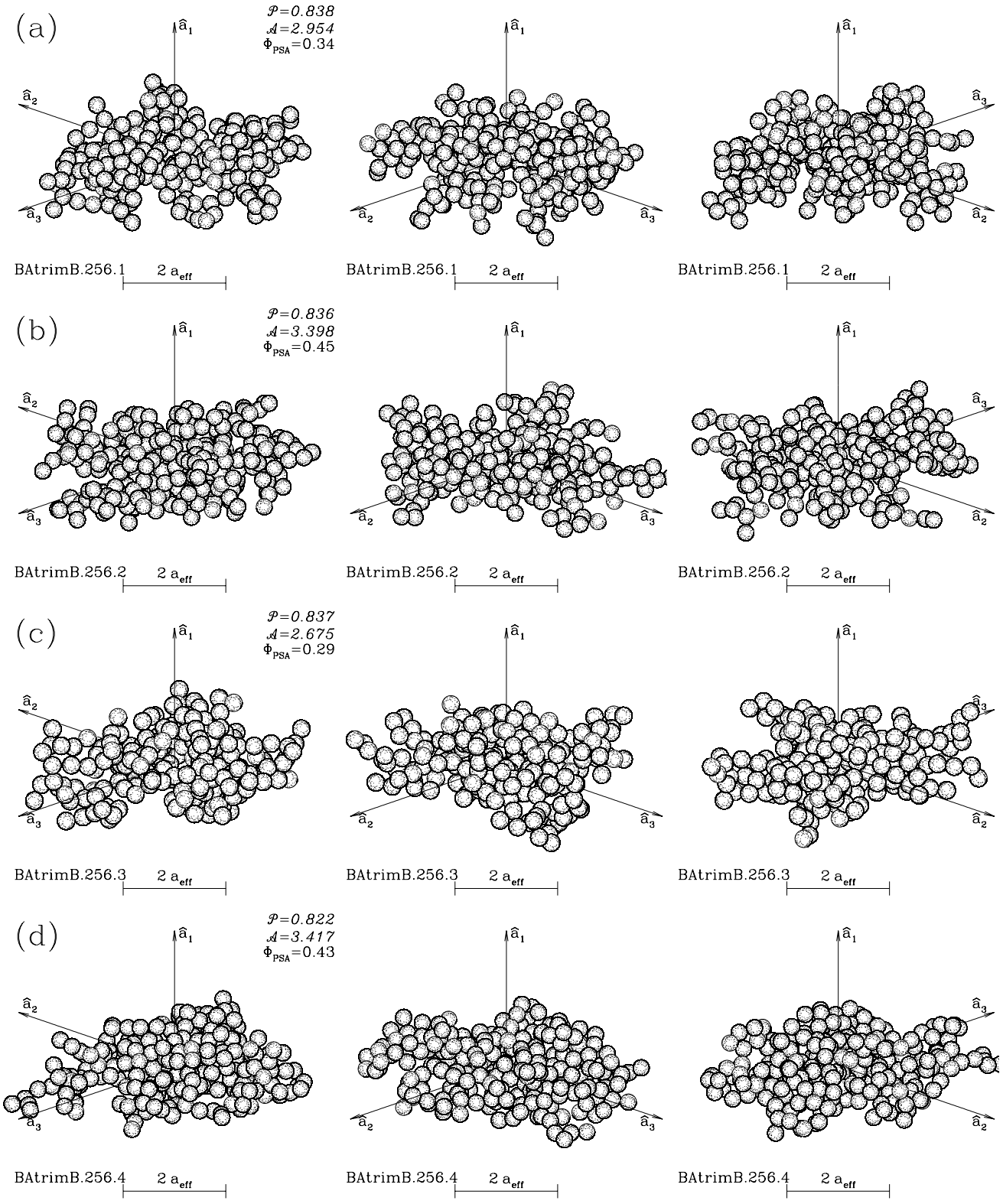

Figure 8. $N = 256$ aggregates obtained from $N = 512$ BA clusters modified by the *trimB* procedure. The BAtrimB.256.3 aggregate consists of only $N = 203$ spheres (see Paper II)

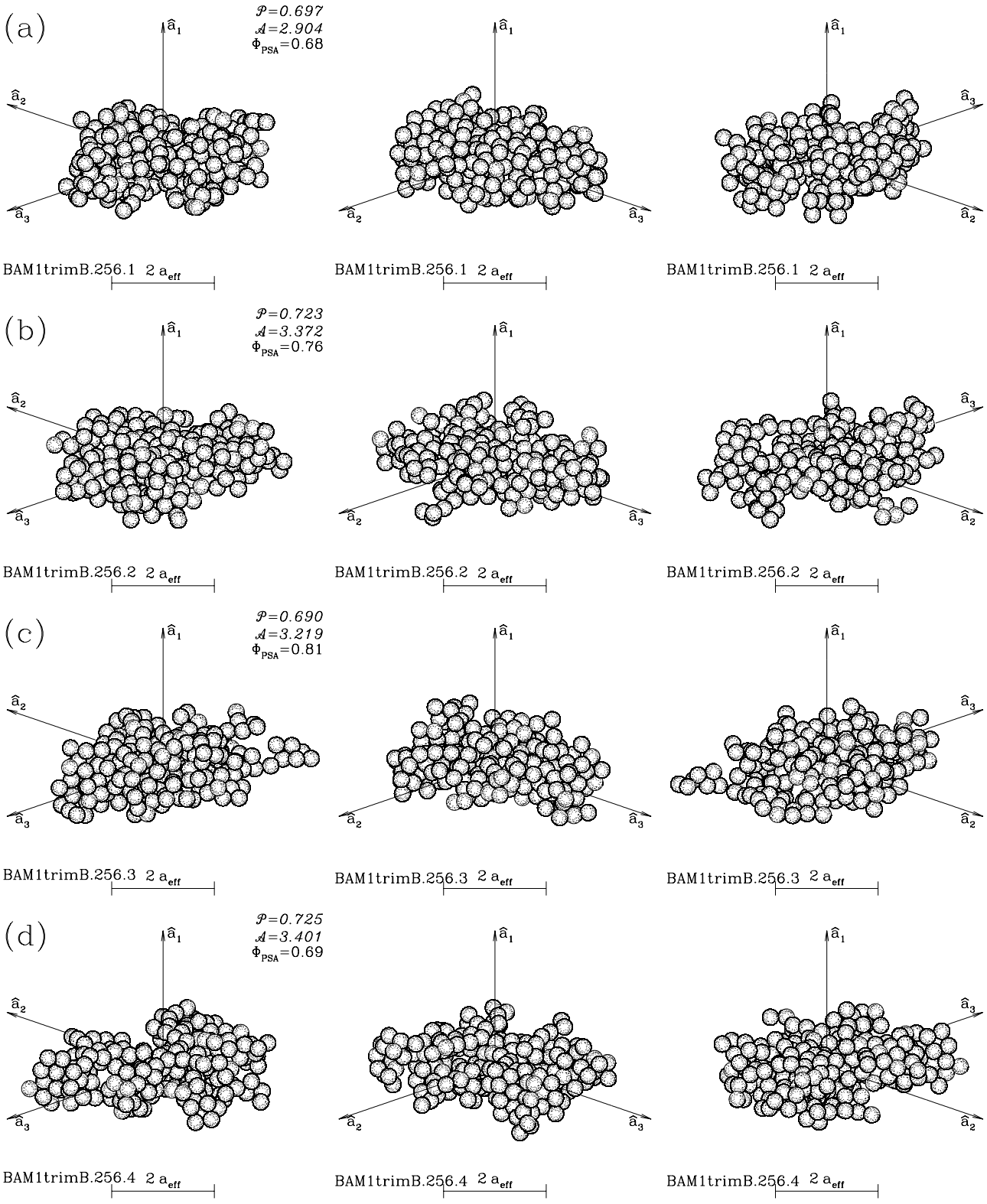

Figure 9. $N = 256$ aggregates obtained from $N = 512$ BAM1 clusters modified by the *trimB* procedure.

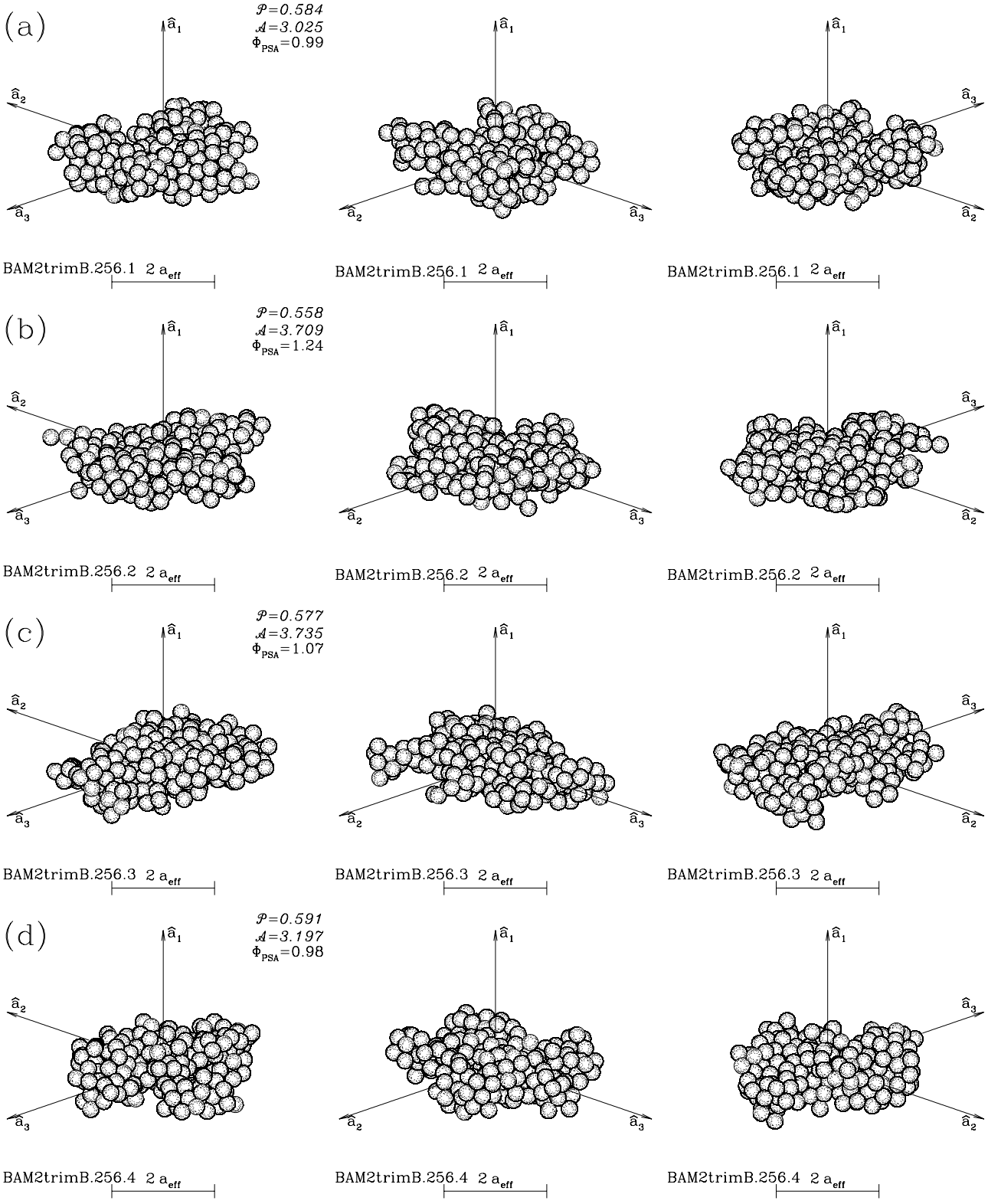

Figure 10. $N = 256$ aggregates obtained from $N = 512$ BAM2 clusters modified by the *trimB* procedure.

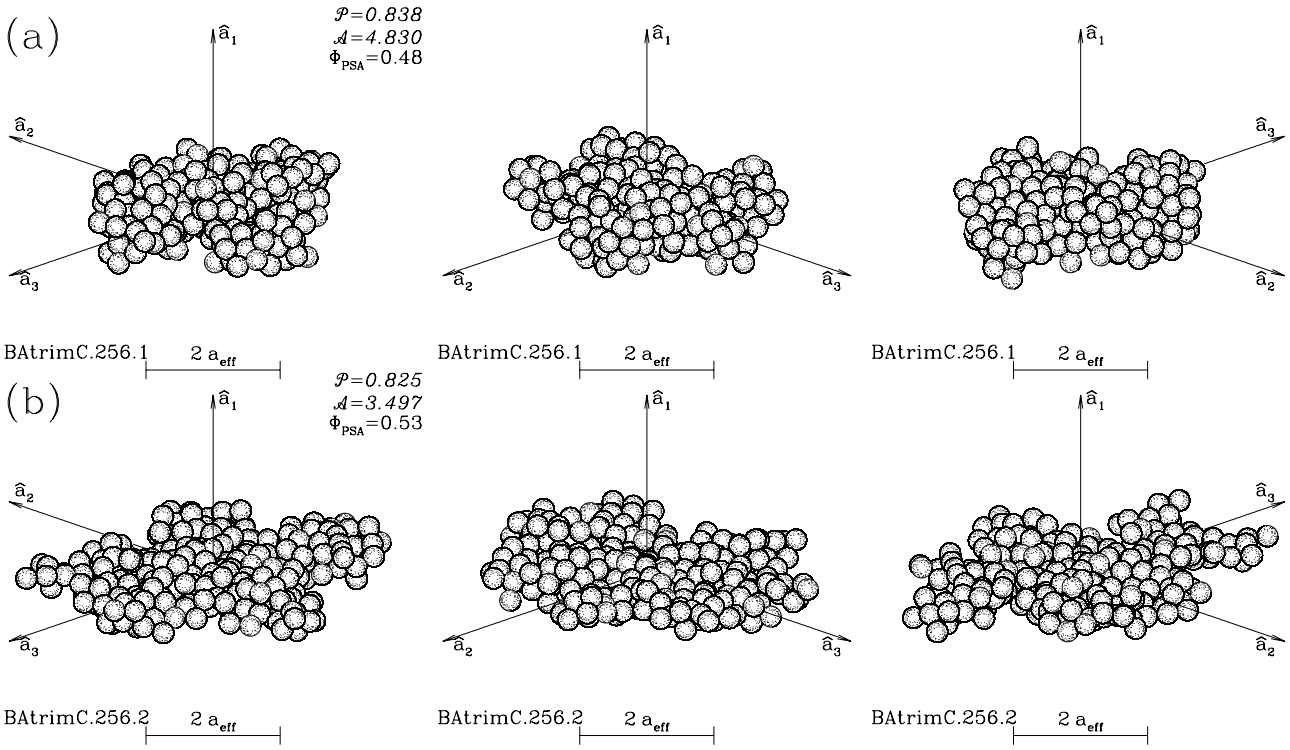

Figure 11. $N = 256$ aggregates obtained from $N = 1024$ BA aggregates modified by the *trimC* procedure.

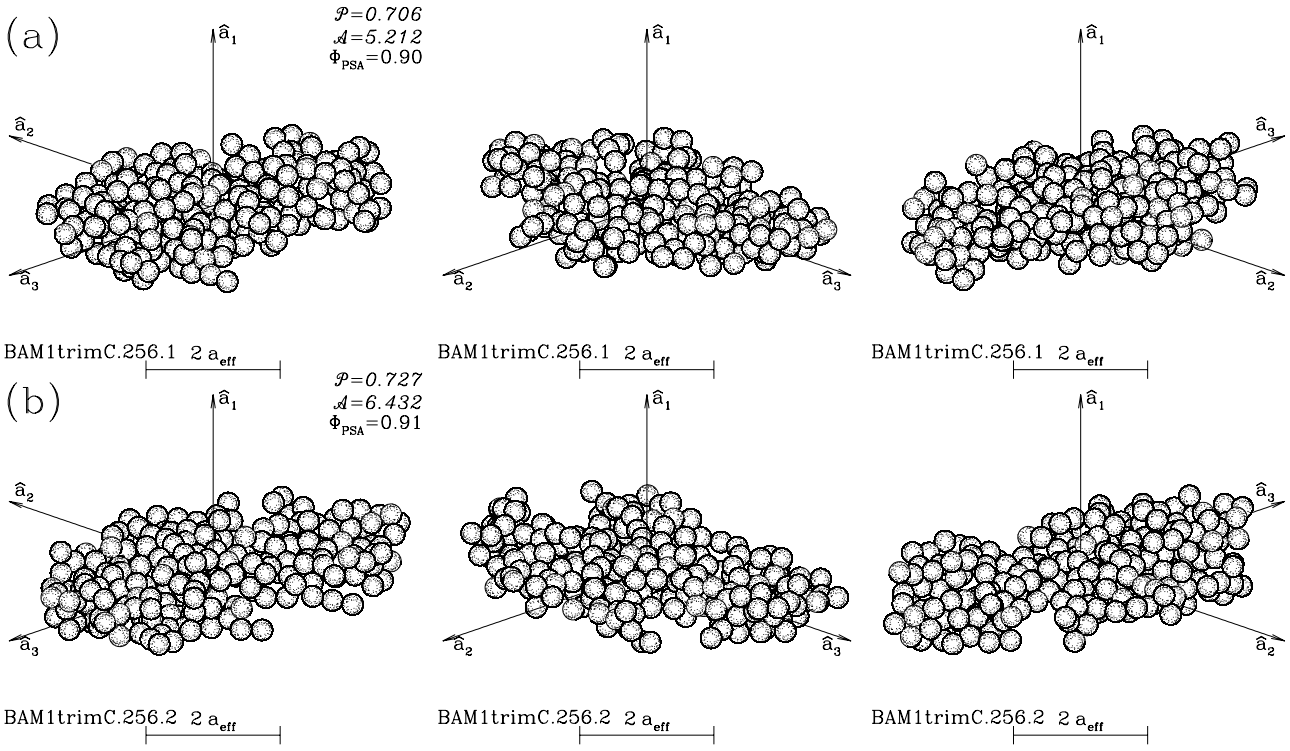

Figure 12. $N = 256$ aggregates obtained from $N = 1024$ BAM1 aggregates modified by the *trimC* procedure.

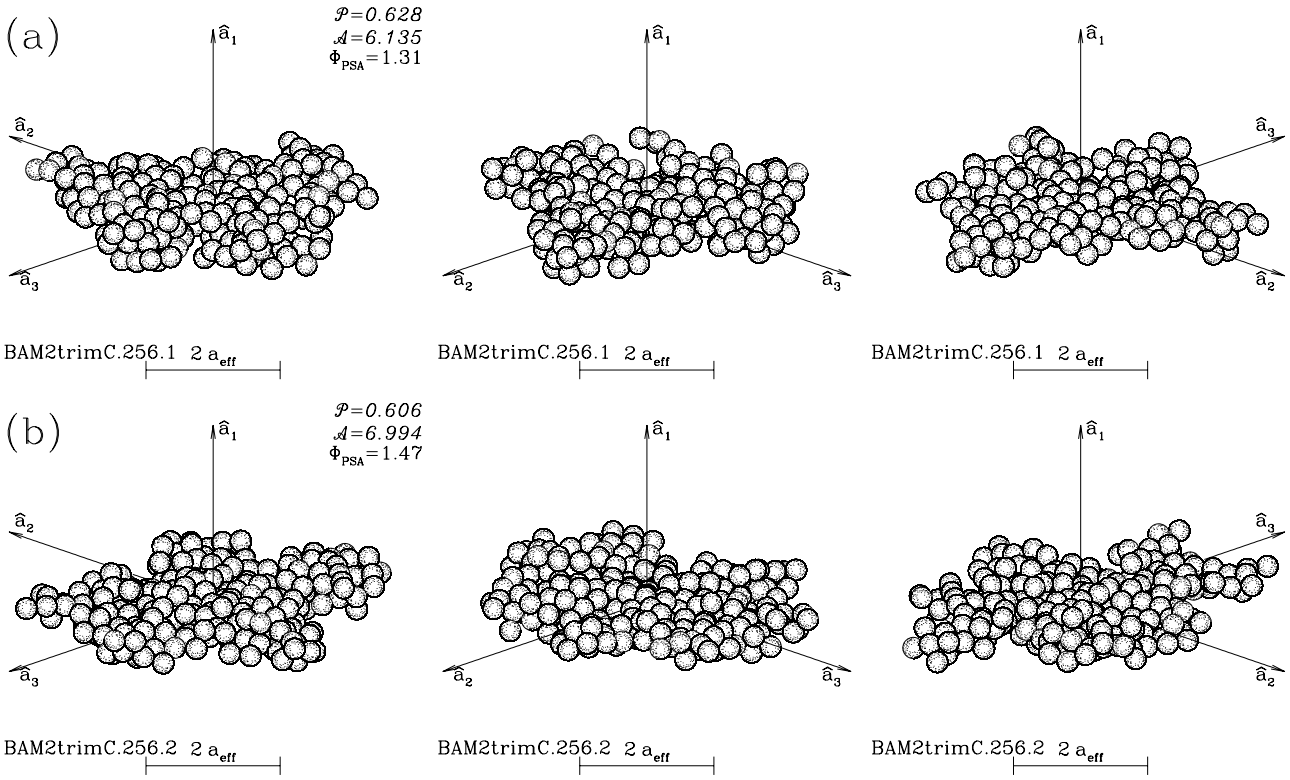

Figure 13. $N = 256$ aggregates obtained from $N = 1024$ BAM2 aggregates modified by the *trimC* procedure.

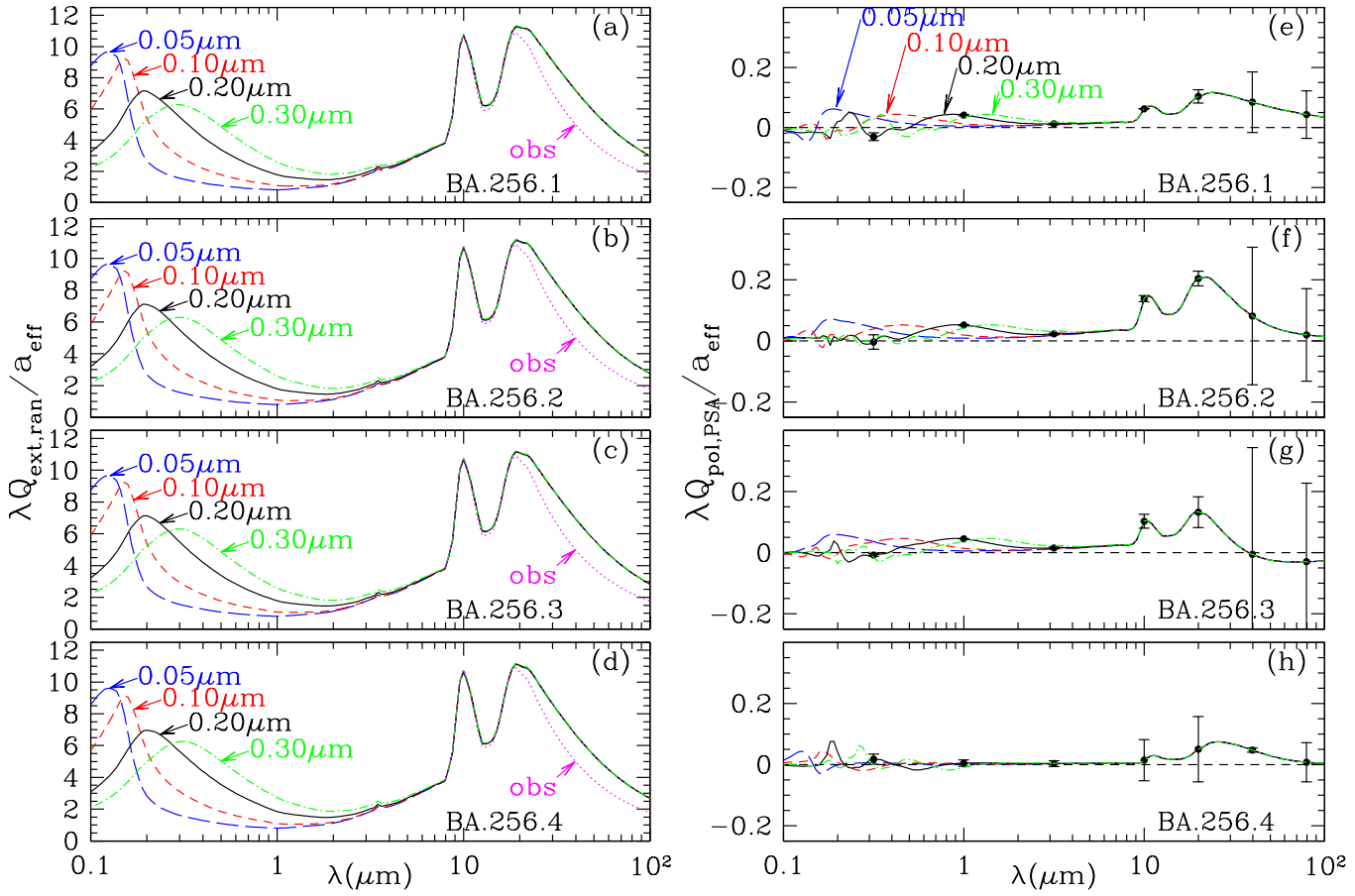

Figure 14. $\lambda Q_{\rm ran}/a_{\rm eff}$ and $\lambda Q_{\rm pol,PSA}/a_{\rm eff}$ for BA aggregates. Dotted line: observed absorption for $\lambda > 8\mu$m. For $a_{\rm eff} = 0.20\mu$m, uncertainties in $\lambda Q_{\rm pol,PSA}/a_{\rm eff}$ are shown at selected wavelengths. *[btd note: fext4ba.pdf, fpol4ba.pdf]*

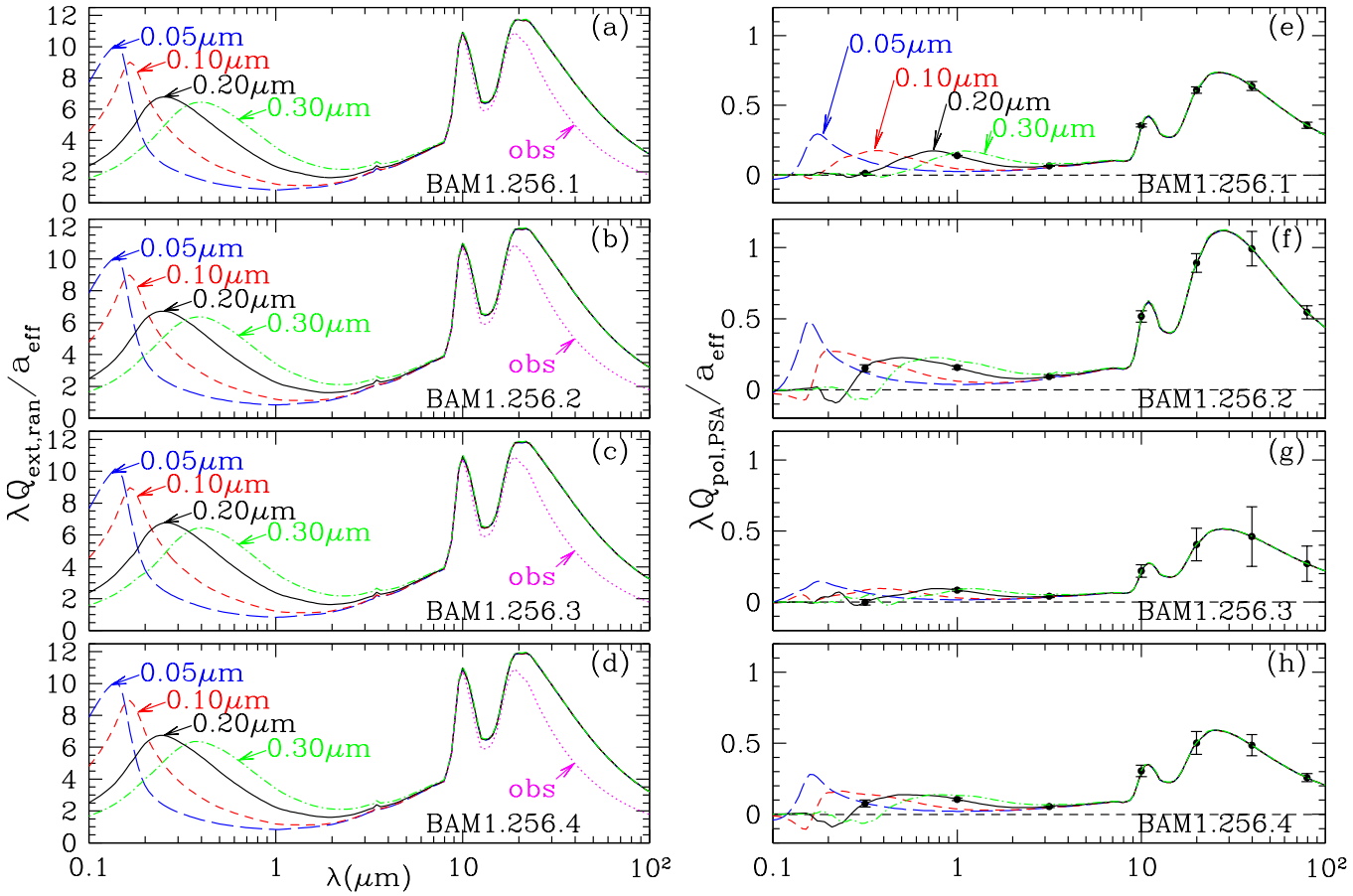

Figure 15. Same as Figure 14, but for BAM1 aggregates. *[btd note: fext4bam1.pdf, fpol4bam1.pdf]*

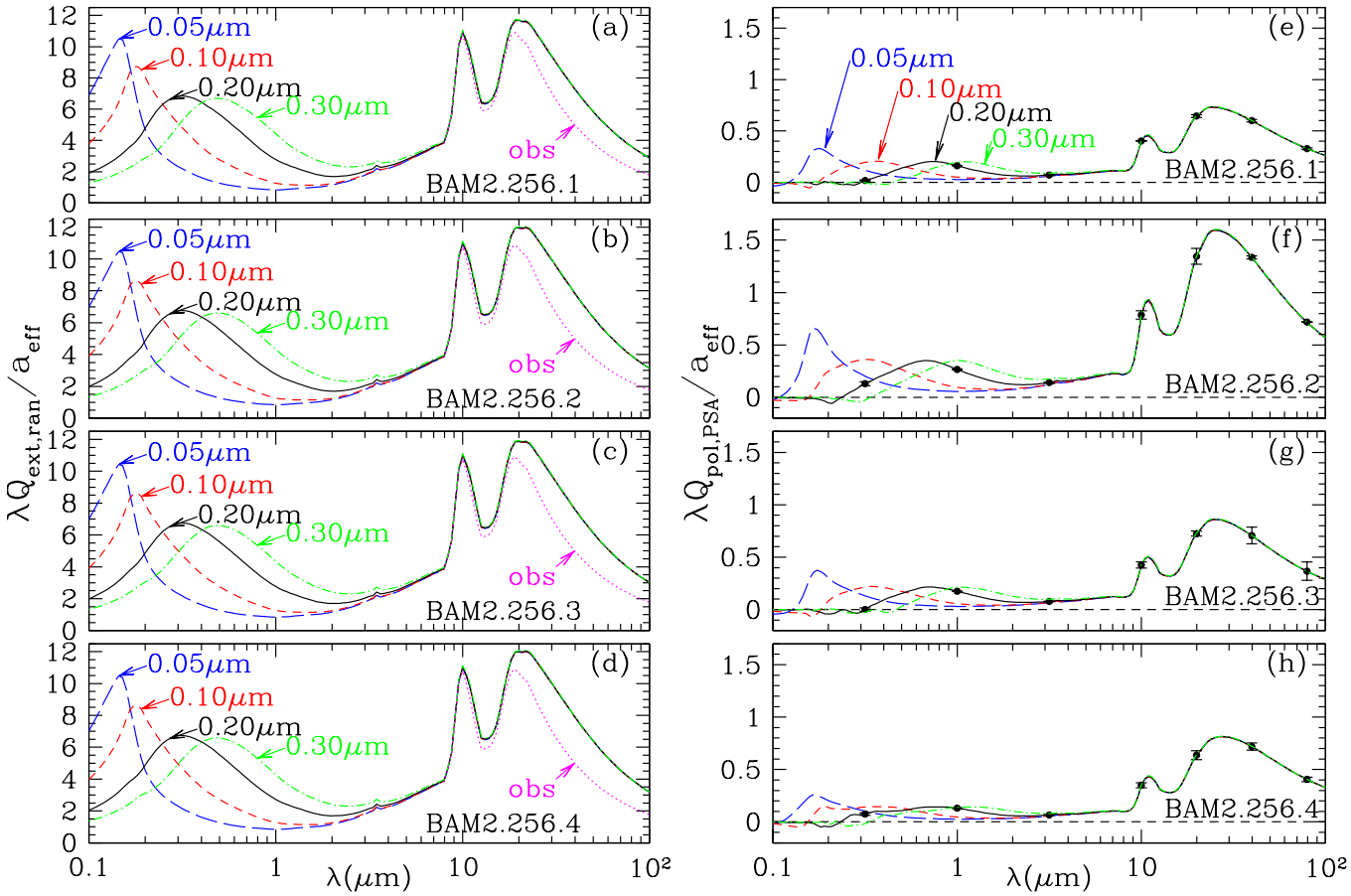

Figure 16. Same as Figure 14, but for BAM2 aggregates. *[btd note: fext4bam2.pdf, fpol4bam2.pdf]*

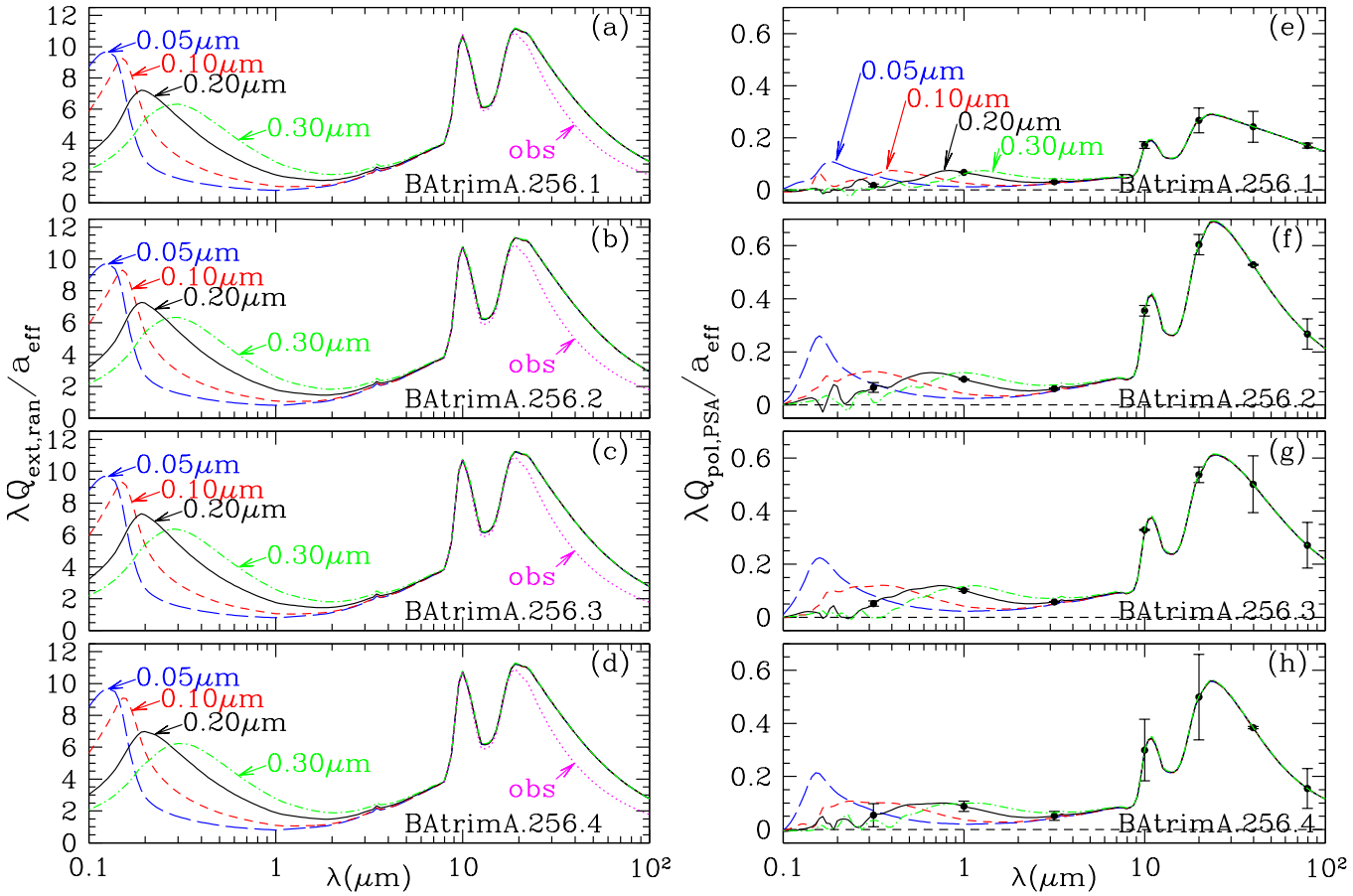

Figure 17. Same as Figure 14, but for BAtrimA aggregates. *[btd note: fext4batrimA.pdf, fpol4batrimA.pdf]*

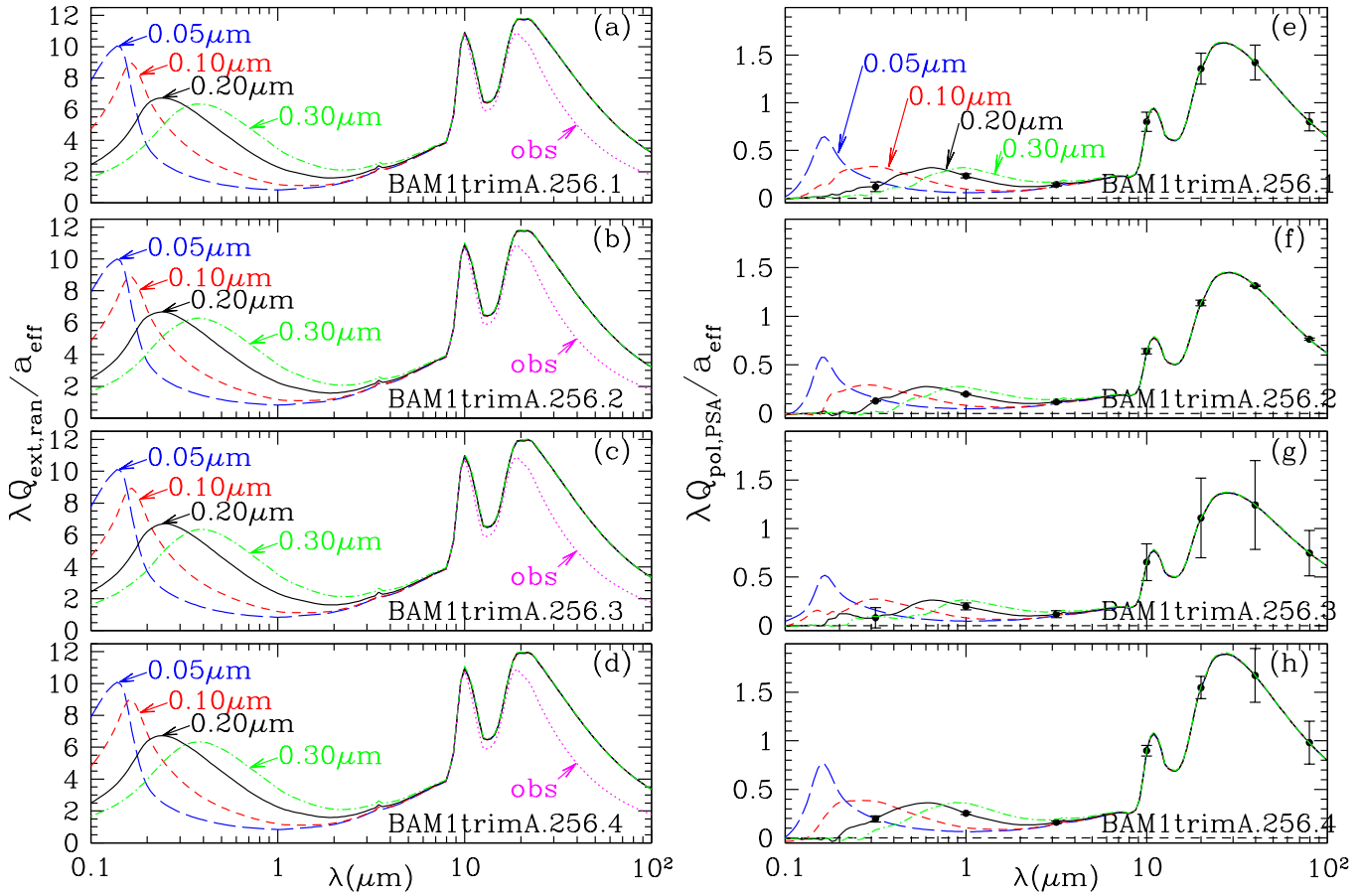

Figure 18. Same as Figure 14, but for BAM1trimA aggregates. *[btd note: fext4bam1trimA.pdf, fpol4bam1trimA.pdf]*

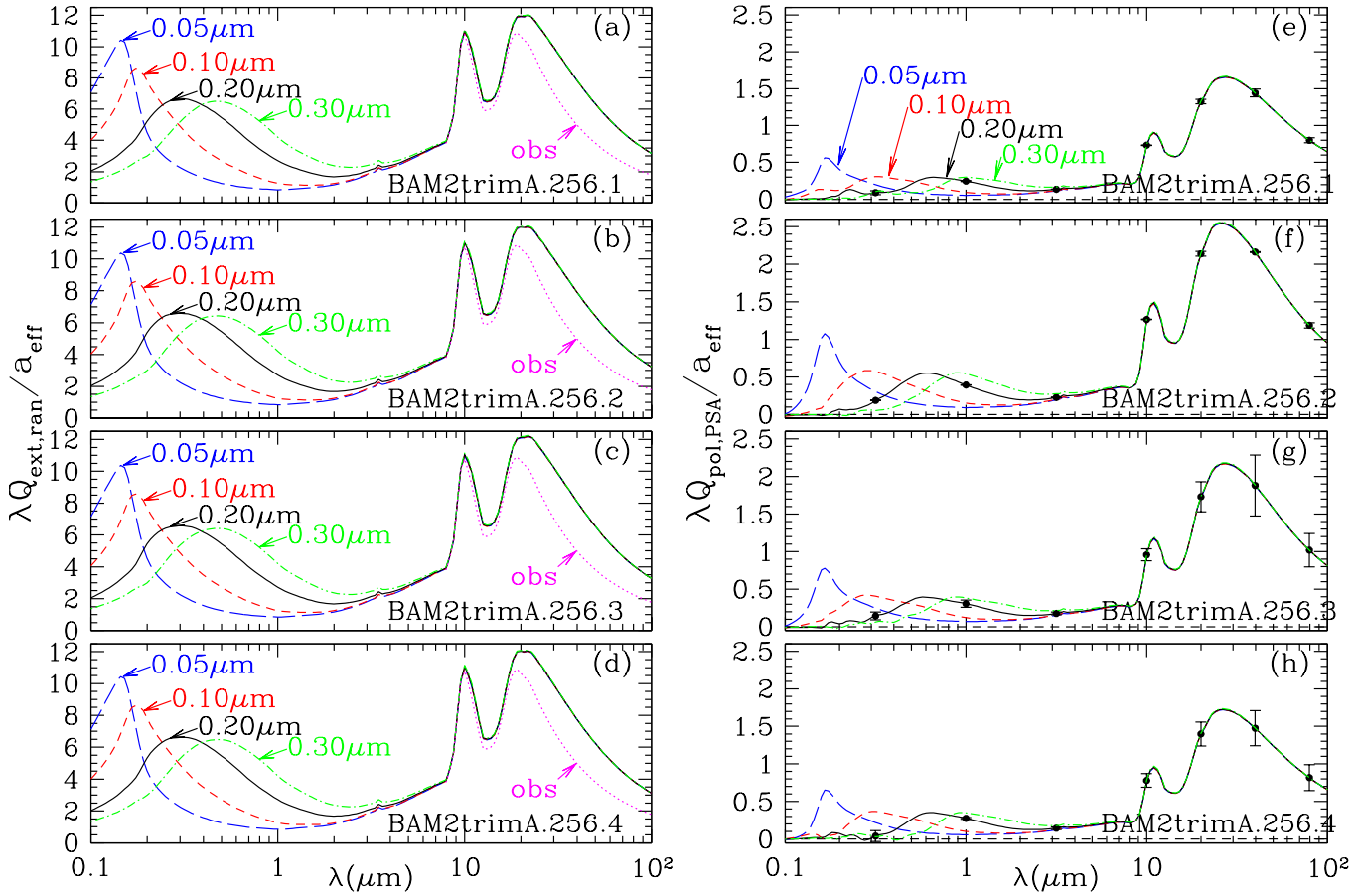

Figure 19. Same as Figure 14, but for BAM2trimA aggregates. *[btd note: fext4bam2trimA.pdf, fpol4bam2trimA.pdf]*

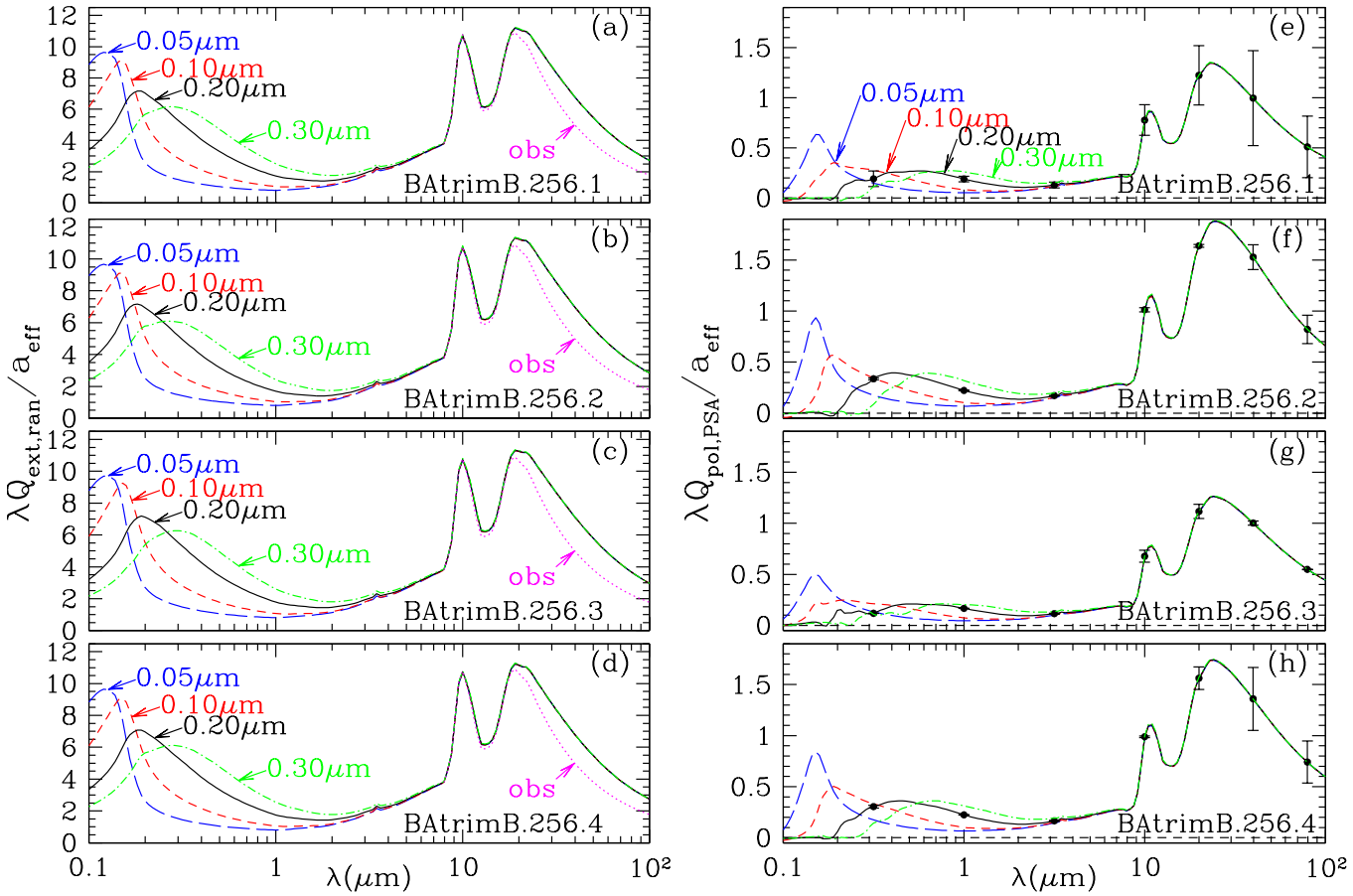

Figure 20. Same as Figure 14, but for BAtrimB aggregates. *[btd note: fext4batrimB.pdf, fpol4batrimB.pdf]*

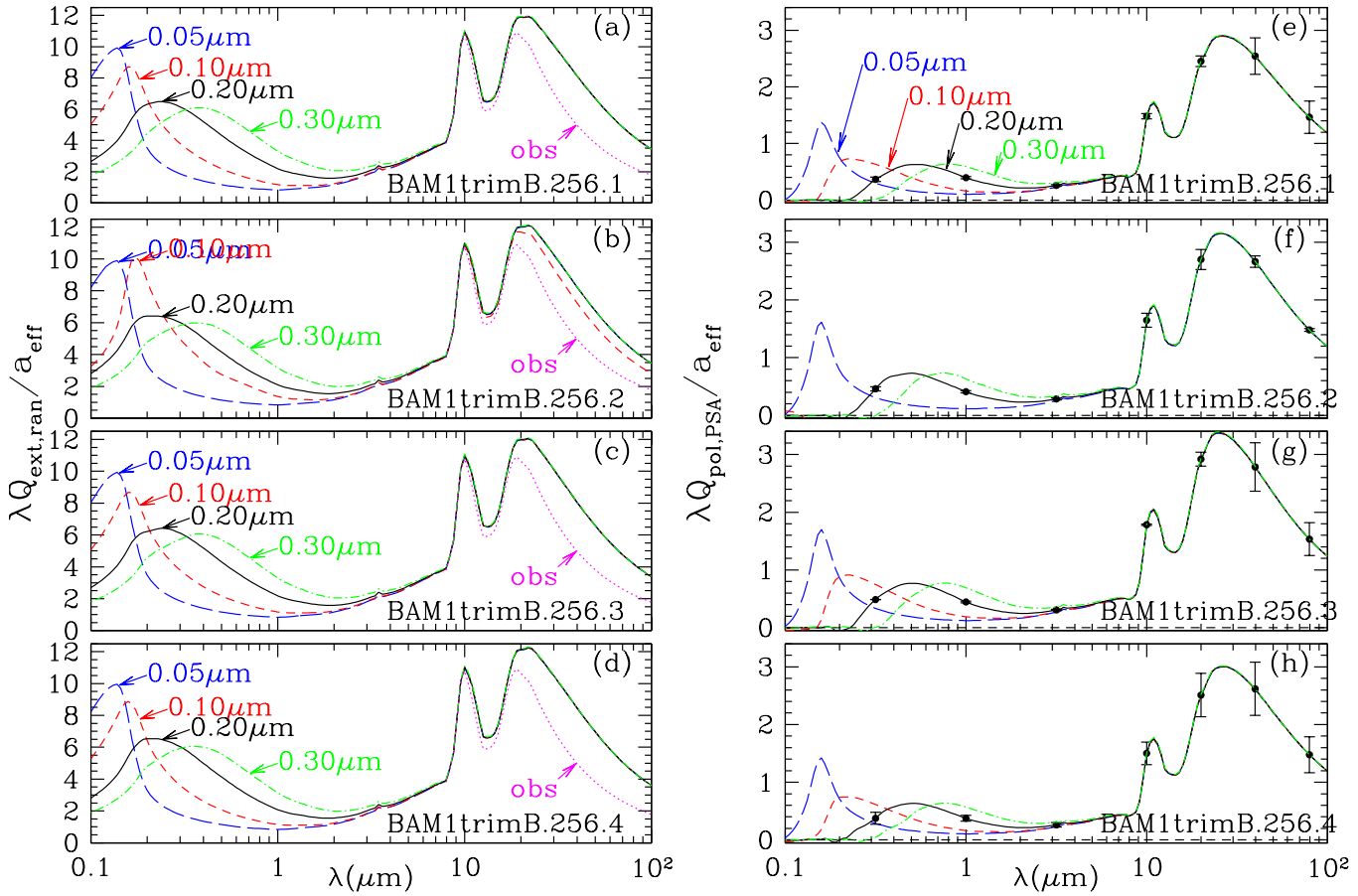

Figure 21. Same as Figure 14, but for BAM1trimB aggregates. *[btd note: fext4bam1trimB.pdf, fpol4bam1trimB.pdf]*

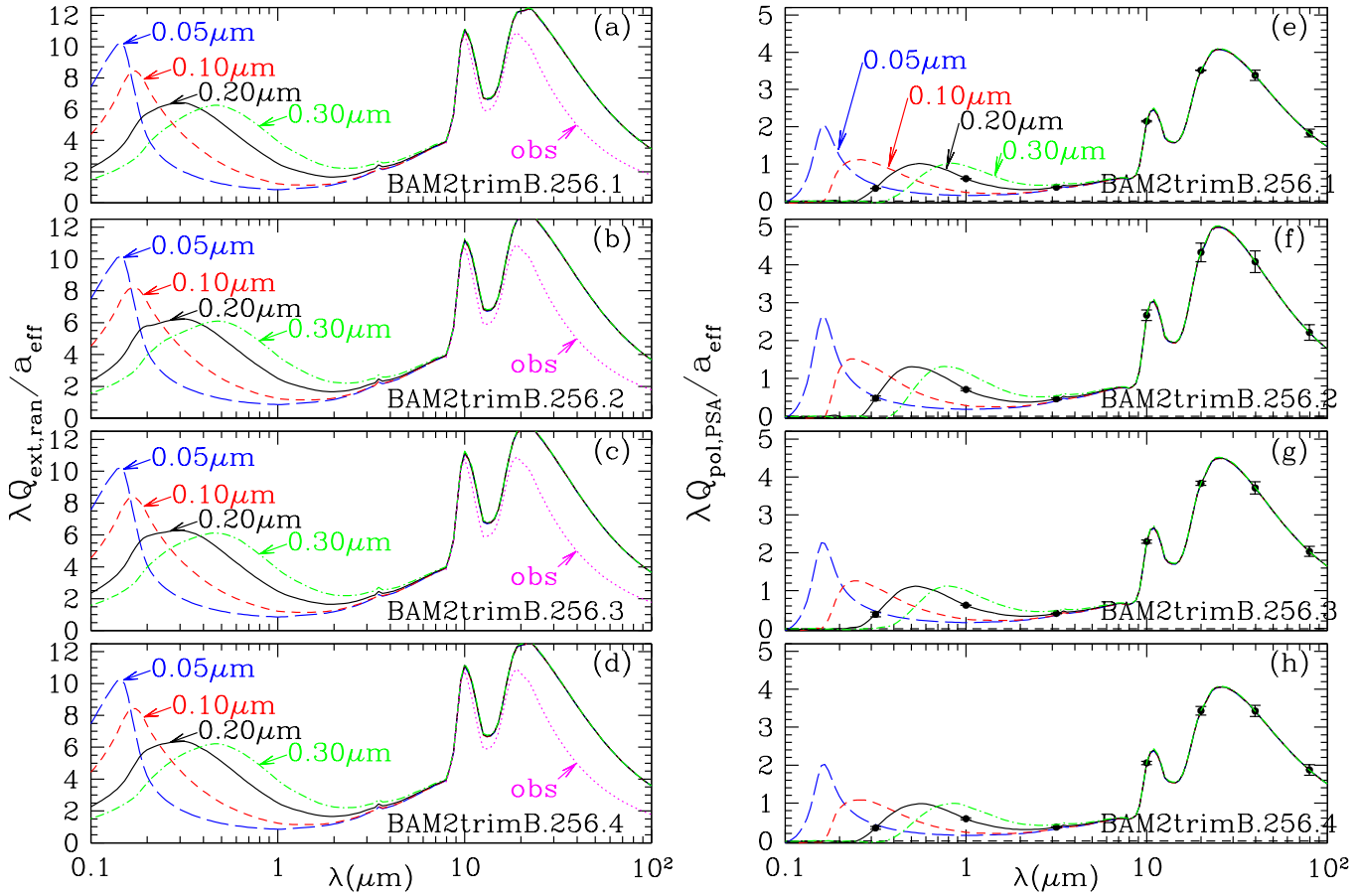

Figure 22. Same as Figure 14, but for BAM2trimB aggregates. *[btd note: fext4bam2trimB.pdf, fpol4bam2trimB.pdf]*

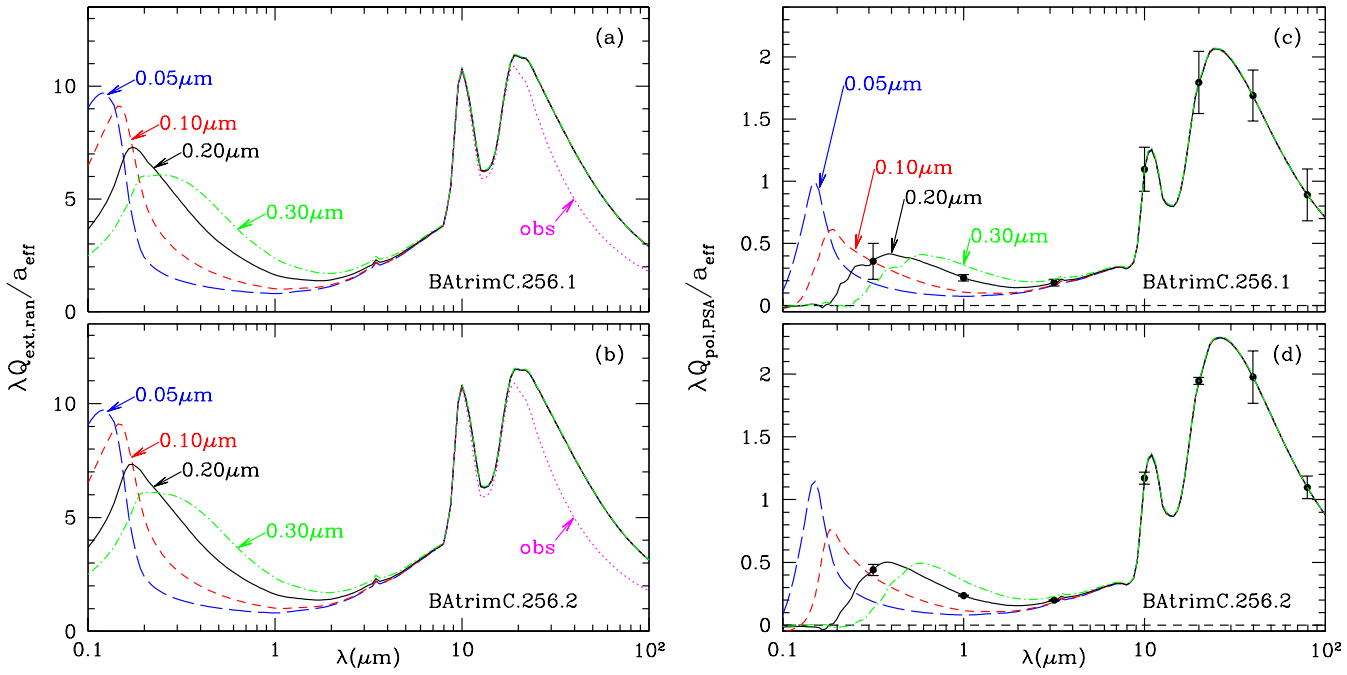

Figure 23. Same as Figure 14, but for BAtrimC aggregates. *[btd note: fext2batrimC.pdf, fpol2batrimC.pdf]*

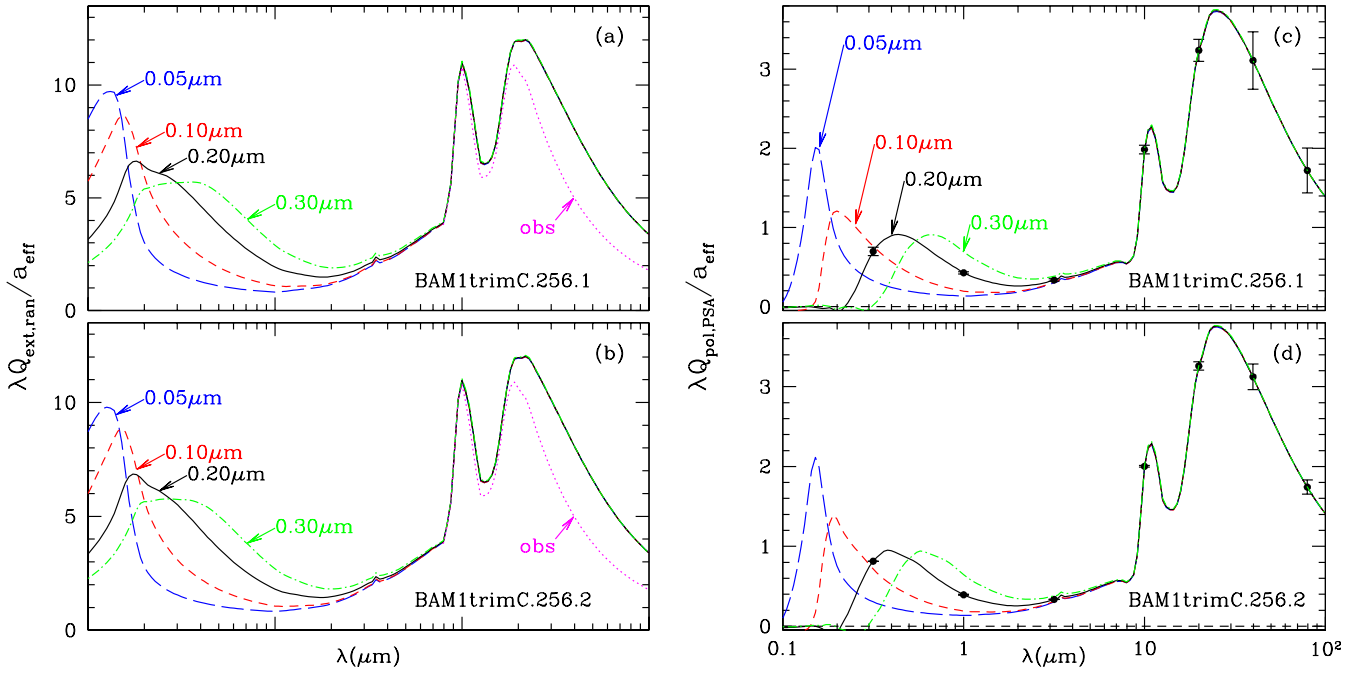

Figure 24. Same as Figure 14, but for BAM1trimC aggregates. *[btd note: fext2bam1trimC.pdf, fpol2bam1trimC.pdf]*

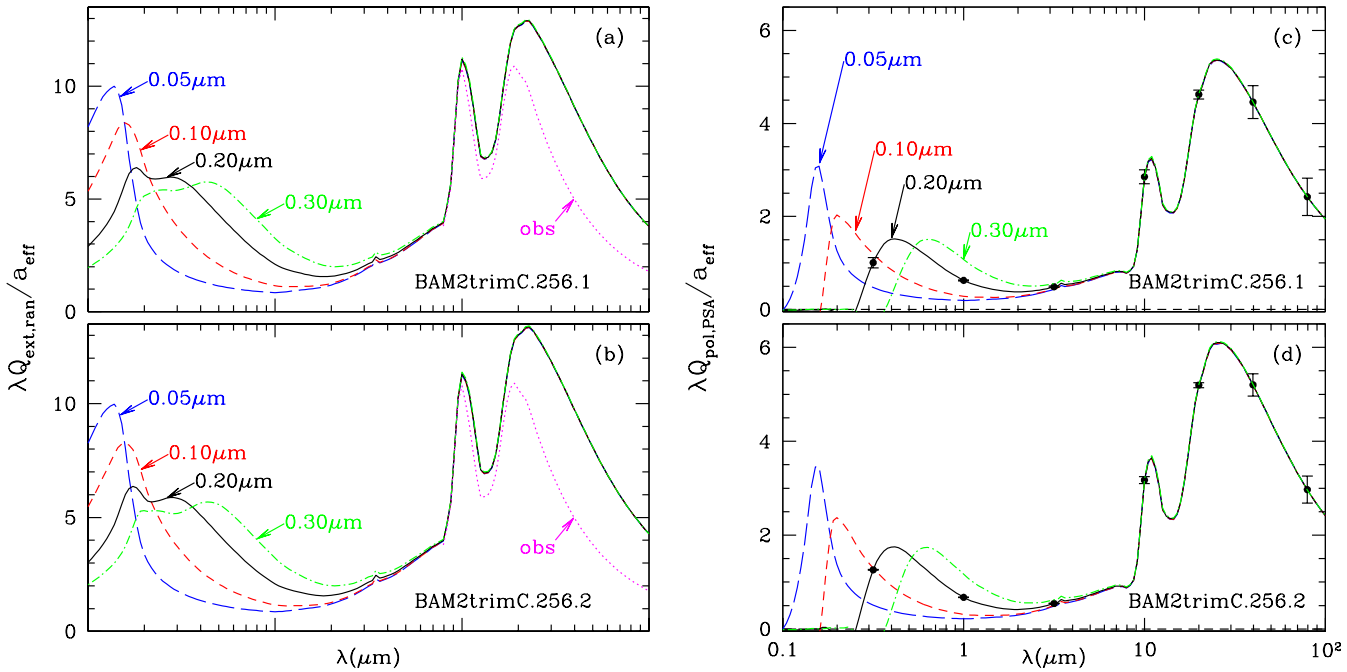

Figure 25. Same as Figure 14, but for BAM2trimC aggregates. *[btd note: fext2bam2trimC.pdf, fpol2bam2trimC.pdf]*